



Production of unknown Fl isotopes in proton evaporation channels within the dinuclear system model

Lu-Qi Li,¹ Gen Zhang ^{1,*} and Feng-Shou Zhang ^{2,3,4}

¹*Guangxi Key Laboratory for Relativistic Astrophysics, School of Physical Science and Technology, Guangxi University, Nanning 530004, China*

²*The Key Laboratory of Beam Technology and Material Modification of Ministry of Education, College of Nuclear Science and Technology, Beijing Normal University, Beijing 100875, China*

³*Beijing Radiation Center, Beijing 100875, China*

⁴*Center of Theoretical Nuclear Physics, National Laboratory of Heavy Ion Accelerator of Lanzhou, Lanzhou 730000, China*



(Received 16 April 2022; accepted 20 July 2022; published 2 August 2022)

The production of Fl isotopes in proton evaporation channels is investigated systematically within the dinuclear system model. Because the proton evaporation is the easiest for Mc isotopes among the isotopes around $Z = 114$, one can synthesize Fl isotopes in the proton evaporation channel. The calculated ER cross sections by the DNS model reproduce the experimental data very well. The dependence of the production cross sections on projectile isospin in capture, fusion, and survival processes in $^{32,34,36}\text{S} + ^{255}\text{Es}$ reactions is studied. The capture cross sections and survival probability in the $^{36}\text{S} + ^{255}\text{Es}$ reaction are the largest, while the fusion probability in the $^{32}\text{S} + ^{255}\text{Es}$ reaction is the highest. The reaction $^{48}\text{Ca} + ^{244}\text{Am}$ is a promising candidate to synthesize the unknown isotope ^{290}Fl with the maximum ER cross section of 4.07 pb in the $p1n$ evaporation channel. Another new isotope ^{291}Fl can be produced in the $^{54}\text{Cr} + ^{239}\text{Pa}$ reaction and the production cross section is estimated to be 0.11 pb.

DOI: [10.1103/PhysRevC.106.024601](https://doi.org/10.1103/PhysRevC.106.024601)

I. INTRODUCTION

The production of new superheavy nuclei has been at the frontier in nuclear physics all the time, which is greatly significant to expanding the nuclear map, exploring the limit of nuclear mass, and studying the structure and properties of exotic nuclei. In recent decades, the synthesis of superheavy nuclei by fusion-evaporation reactions has made great progress in experiments [1–18]. The superheavy nuclei with $Z < 113$ have been produced in the cold fusion reactions based on the ^{208}Pb or ^{209}Bi target [1–5], while the hot fusion reactions with a ^{48}Ca beam have been applied to synthesize the heavier elements up to $Z = 118$ [6–18]. Since the stability line bends to the neutron axis, the superheavy nuclei synthesized by fusion reactions are neutron-deficient, and the yields decrease rapidly with the increasing atomic number of the compound nuclei.

According to the predictions of the theoretical models [19–22], the center of the island of stability is most likely located at $Z = 114$ and $N = 184$. The nuclei on the island of stability are expected to have particular properties, such as high binding energy, long half-life, strong shell effect, and so on. The interest in synthesizing Fl isotopes is motivated by the predictions of the island of stability. Until now, only six Fl isotopes have been synthesized in the experiment [7,23–26]. $^{284,286-289}\text{Fl}$ were synthesized with the cross sections at

the level of 1 pb at Dubna employing the DGFRS [27]. The $^{48}\text{Ca} + ^{244}\text{Pu}$ reaction was applied to produce the isotopes $^{288-289}\text{Fl}$, and the target ^{242}Pu was chosen to produce $^{286-287}\text{Fl}$. Only one Fl isotope, ^{285}Fl , was produced at LBNL (Lawrence Berkeley National Laboratory), with a cross section only 0.6 pb. In 2015, the most neutron-deficient Fl isotope, ^{284}Fl , was generated in $^{48}\text{Ca} + ^{239,240}\text{Pu}$ reactions. The Fl isotopes synthesized in the experiment are all neutron-deficient, and ^{289}Fl has the most neutrons with nine fewer neutrons compared with the center of island of stability.

In order to describe the fusion mechanism in heavy-ion collisions [28–30], many theoretical models have been developed. The semiclassical models include dinuclear system (DNS) model [31–36], two-step model [37], nuclear collectivization model [38], the fusion-by-diffusion model [39], and multidimensional Langevin-type dynamical equations [40]. In addition, the microscopic models, such as the time-dependent Hartree-Fock (TDHF) model [41] and the improved quantum molecular dynamics (ImQMD) model [42,43], can simulate the dynamical evolution of fusion processes very well. The DNS model can describe the mass and charge diffusion of the dinuclear system, and the dissipation of kinetic energy and angular momentum, which is successful to predict the production cross sections of superheavy nuclei in fusion evaporation reactions.

It is very difficult to approach the island of stability only considering the neutron evaporation channels in the de-excitation processes of the compound nuclei. In this work, the statistical evaporation model is improved to deal with

*Corresponding author: zhanggen@gxu.edu.cn

charged particle evaporation, especially the proton evaporation channel, to produce the FI isotopes to access the island of stability. Considering proton evaporation channels can not only produce more neutron-rich isotopes but also provide more choices of projectile-target combinations for the experiments. In previous studies, the evaporation of protons is generally ignored due to the high Coulomb barrier. Nevertheless, if the daughter nucleus has a higher fission barrier than the parent nucleus after the emission of protons, the survival probability can be large, so the evaporation residual cross sections in proton evaporation channels should be comparable.

The article is organized as follows. In Sec. II, the DNS model is introduced briefly. The calculated results and discussion are shown in Sec. III. Finally, the main conclusion is given in Sec. IV.

$$T(E_{c.m.}, J) = \int f(B) \times \frac{1}{1 + \exp\left\{-\frac{2\pi}{\hbar\omega(J)}\left[E_{c.m.} - B - \frac{\hbar^2}{2\mu R_B^2(J)}J(J+1)\right]\right\}} dB. \quad (2)$$

Here, $\hbar\omega$ is the width of the parabolic barrier and R_B defines the position of the barrier. Considering the multidimensional character of the realistic barrier, the barrier distribution function $f(B)$ should be introduced, which is taken as the asymmetric Gaussian form [38].

From the viewpoint of the DNS concept, the nucleon transfer occurs at the bottom of the potential pocket after the colliding nuclei overcome the Coulomb barrier. Fusion can lead to the formation of the compound nucleus, competing with the quasifission process at this stage. The nucleon transfer process is governed by the potential energy surface (PES), which is given by the following formula [31,45]:

$$U(Z_1, N_1, Z_2, N_2, R) = \Delta(Z_1, N_1) + \Delta(Z_2, N_2) + V_C(Z_1, N_1, Z_2, N_2, R) + V_N(Z_1, N_1, Z_2, N_2, R), \quad (3)$$

where $\Delta(Z_1, N_1)$ and $\Delta(Z_2, N_2)$ indicate the mass excesses of both fragments. R is the distance between both fragments at the bottom of the potential pocket. The Coulomb potential V_C and nuclear potential V_N are calculated by the Wong formula [46] and the double folding method [47], respectively.

The distribution probability $P(Z_1, N_1, t)$ for the fragment with proton number Z_1 and neutron number N_1 at time t is determined by solving the master equation [48,49]

$$\begin{aligned} \frac{dP(Z_1, N_1, t)}{dt} = & \sum_{Z'_1} W_{Z_1, N_1; Z'_1, N_1}(t) [d_{Z_1, N_1} P(Z'_1, N_1, t) \\ & - d_{Z'_1, N_1} P(Z_1, N_1, t)] \\ & + \sum_{N'_1} W_{Z_1, N_1; Z_1, N'_1}(t) [d_{Z_1, N_1} P(Z_1, N'_1, t) \\ & - d_{Z_1, N'_1} P(Z_1, N_1, t)] \\ & - [\Lambda_{qf}(\Theta(t)) + \Lambda_{fis}(\Theta(t))] P(Z_1, N_1, t), \quad (4) \end{aligned}$$

where d_{Z_1, N_1} represents the microscopic dimension corresponding to the macroscopic state (Z_1, N_1) of the fragment. Λ_{qf} and Λ_{fis} are the quasifission and fission rates, respectively, which are calculated by the one-dimensional Kramers equation [50,51]. $W_{Z_1, N_1; Z'_1, N_1}(W_{Z_1, N_1; Z_1, N'_1})$ is the transition probability from channel (Z_1, N_1) to (Z'_1, N_1) [or from (Z_1, N_1) to (Z_1, N'_1)], which can be written

II. THE MODEL

Within the framework of DNS, the evaporation residue (ER) cross sections of superheavy nuclei at the incident energy $E_{c.m.}$ are calculated by [35]

$$\begin{aligned} \sigma_{ER}(E_{c.m.}) = & \frac{\pi \hbar^2}{2\mu E_{c.m.}} \sum_{J=0}^{J_{\max}} (2J+1) T(E_{c.m.}, J) \\ & \times P_{CN}(E_{c.m.}, J) W_{sur}(E_{c.m.}, J). \quad (1) \end{aligned}$$

Here, T , P_{CN} , and W_{sur} are the transmission, fusion, and survival probability, respectively.

The transmission probability under the parabolic approximation can be written as [44]

as

$$\begin{aligned} W_{Z_1, N_1; Z'_1, N_1}(t) = & \frac{\tau_{mem}(Z_1, N_1, E_1, Z'_1, N_1, E'_1; t)}{\hbar^2 d_{Z_1, N_1} d_{Z'_1, N_1}} \\ & \times \sum_{ii'} | \langle Z'_1, N_1, E'_1, i' | V(t) | Z_1, N_1, E_1, i \rangle |^2. \quad (5) \end{aligned}$$

Here, τ_{mem} is the memory time and i represents the remaining quantum numbers.

The fusion probability is taken as the sum of the distribution probability of the fragments passing over the Businaro Gallone (BG) point:

$$P_{CN}(E_{c.m.}, J, B) = \sum_{Z_1=1}^{Z_{BG}} \sum_{N_1=1}^{N_{BG}} P(Z_1, N_1, \tau_{int}(J, B)), \quad (6)$$

where τ_{int} denotes the interaction time, calculated by the deflection function method [52]. Z_{BG} and N_{BG} represent the proton number and neutron number at the BG point, respectively. Considering the distribution of the Coulomb barrier, the fusion probability can be written as

$$P_{CN}(E_{c.m.}, J) = \int f(B) P_{CN}(E_{c.m.}, J, B) dB. \quad (7)$$

The compound nucleus with high excitation energy and angular momentum de-excites by the emission of γ rays, light particles (such as neutrons, protons, α particles, and so on), and fission. The competition among various de-excitation

modes can be characterized by the evaporation width. In the previous theoretical studies on the synthesis of superheavy nuclei, only the competition between neutron evaporation and fission is treated. In this work, the contribution from proton evaporation was added to the de-excitation process.

According to Weisskopf's evaporation theory [53], the evaporation width of particle ν can be written as

$$\Gamma_\nu(E^*, J) = (2s_\nu + 1) \frac{m_\nu}{\pi^2 \hbar^2 \rho(E^*, J)} \times \int_0^{E^* - B_\nu - \delta - \delta_n - \frac{1}{a}} \varepsilon \rho(E^* - B_\nu - \delta_n - \varepsilon) \sigma_{\text{inv}}(\varepsilon) d\varepsilon, \quad (8)$$

where s_ν , m_ν , and B_ν are the spin, mass, and binding energy of the particle, respectively. The pairing correction δ is set to be $12/\sqrt{A}$, 0, and $-12/\sqrt{A}$ for even-even, odd- A , and odd-odd

$$\Gamma_f(E^*, J) = \frac{1}{2\pi \rho_f(E^*, J)} \times \int_0^{E^* - B_f - \delta - \delta_f - \frac{1}{a_f}} \frac{\rho(E^* - B_f - \delta_f - \varepsilon) d\varepsilon}{1 + \exp[-2\pi(E^* - B_f - E_{\text{rot}} - \varepsilon)/\hbar\omega]}. \quad (12)$$

In this work, the statistical model is extended to describe the proton evaporation during the de-excitation process of a highly excited compound nucleus. The survival probability of a superheavy nucleus with excitation energy E_{CN}^* and angular momentum J in x -proton and y -neutron evaporation channel can be expressed as [55–57]

$$W_{\text{sur}}(E_{\text{CN}}^*, x, y, J) = P(E_{\text{CN}}^*, x, y, J) \prod_{i=1}^x \frac{\Gamma_p(E_i^*, J)}{\Gamma_{\text{tot}}(E_i^*, J)} \times \prod_{j=x+1}^{x+y} \frac{\Gamma_n(E_j^*, J)}{\Gamma_{\text{tot}}(E_j^*, J)}, \quad (13)$$

where $\Gamma_{\text{tot}} = \Gamma_n + \Gamma_p + \Gamma_f$. $P(E_{\text{CN}}^*, x, y, J)$ is the realization probability, which is given by the Jackson formula [58]. E_i^* is the excitation energy before evaporating the i th particle, which can be calculated from the equation $E_{i+1}^* = E_i^* - B_i^\nu - 2T_i$. B_i^ν is the separation energy of the i th particle. In particular, if protons are evaporated, V_p 's contribution to separation energy should be considered [59]. T_i is nuclear temperature before the i th particle evaporated, obtained from $T_i = \sqrt{E_i^*/a}$.

III. RESULTS AND DISCUSSION

To evaluate the strength of proton evaporation for superheavy nuclei near $Z = 114$, a ratio $R = B_f/(B_p + V_c)$ is defined to describe the competition between proton evaporation and fission. Here, B_f , B_p , and V_c represent the fission barrier, proton binding energy, and the barrier for proton evaporation, respectively. The R ratios of the isotopes $^{286-297}\text{Nh}$, $^{286-297}\text{Fl}$, $^{285-296}\text{Mc}$, and $^{286-297}\text{Lv}$ are shown in Fig. 1, denoted by squares, circles, pentagons, and triangles, respectively. It can be seen that the ratios of $^{285-296}\text{Mc}$ are the largest while the ratios of $^{286-297}\text{Fl}$ are the smallest, meaning that proton evaporation is the easiest for Mc isotopes but the most difficult for Fl isotopes due to the proton closed-shell at $Z = 114$.

nuclei, respectively. ρ is the energy level density, derived from the Fermi-gas model.

The reverse cross section σ_{inv} is given by the following formula:

$$\sigma_{\text{inv}}(\varepsilon) = \begin{cases} \pi R_\nu^2 (1 - \frac{V_\nu}{\varepsilon}), & \varepsilon > V_\nu \\ 0, & \varepsilon < V_\nu \end{cases}, \quad (9)$$

where R_ν can be expressed as

$$R_\nu = 1.16[(A - A_\nu)^{1/3} + A_\nu^{1/3}]. \quad (10)$$

Here, A_ν is the mass number of the evaporated particle. For proton evaporation, the Coulomb barrier V_p is parametrized by the following formula [55]:

$$V_p = [1.15Z_\nu(Z - Z_\nu)]/(R_\nu + 1.6). \quad (11)$$

The fission decay width can be calculated within the Bohr-Wheeler transition-state method [54]:

That hints that one can synthesize the compound nuclei of Mc first, then approach the Fl isotopes in the proton evaporation channel. As a test of the DNS model, the comparisons of calculated ER cross sections with the experimental data in the reactions $^{48}\text{Ca} + ^{243}\text{Am}$, $^{48}\text{Ca} + ^{248}\text{Cm}$, $^{48}\text{Ca} + ^{249}\text{Bk}$, and $^{48}\text{Ca} + ^{249}\text{Cf}$ are shown in Fig. 2. The solid, dashed, and dash-dotted lines represent the calculated ER cross sections in $2n$, $3n$, and $4n$ evaporation channels, respectively. The triangles, squares, and circles represent the experimental data in $2n$, $3n$, and $4n$ evaporation channels, respectively [24,25,60,61]. One can see that the calculated results are in a good agreement with the experimental ones within the error bars. As the charge number of the superheavy nuclei becomes larger, the experimental ER cross sections decrease rapidly, and the calculated results show the same trend. For the peak positions which are

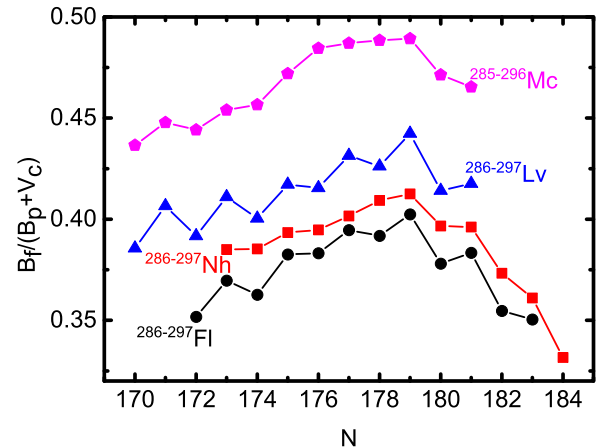


FIG. 1. The ratios $R = B_f/(B_p + V_c)$ of nuclei $^{286-297}\text{Nh}$, $^{286-297}\text{Fl}$, $^{285-296}\text{Mc}$, and $^{286-297}\text{Lv}$ are denoted by the squares, circles, pentagons, and triangles, respectively.

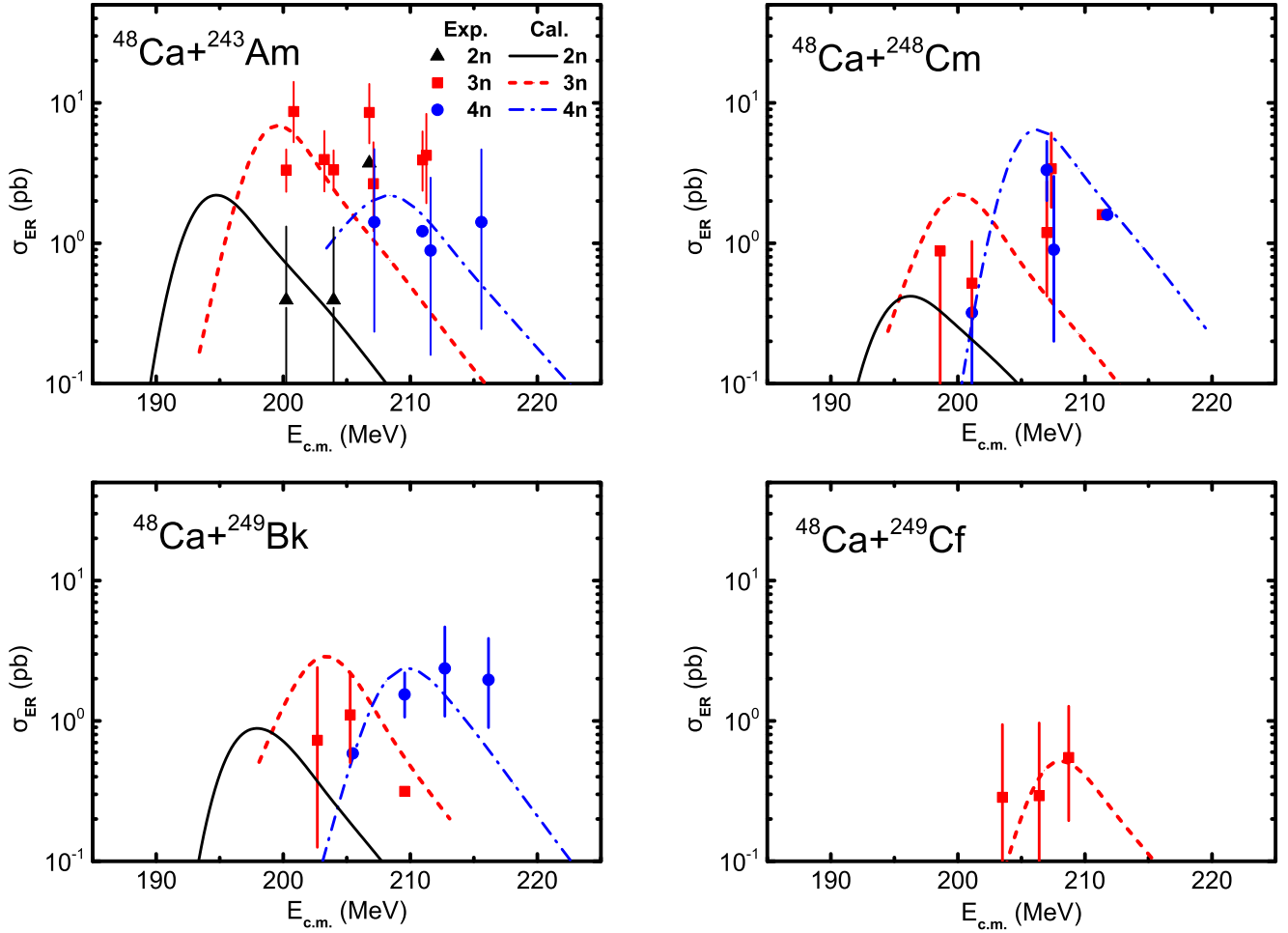


FIG. 2. Comparisons of calculated ER cross sections with the experimental data in $^{48}\text{Ca} + ^{243}\text{Am}$, $^{48}\text{Ca} + ^{248}\text{Cm}$, $^{48}\text{Ca} + ^{249}\text{Bk}$, and $^{48}\text{Ca} + ^{249}\text{Cf}$ reactions. The solid, dashed, and dash-dotted lines represent the calculated ER cross sections in $2n$, $3n$, and $4n$ evaporation channels, respectively. The triangles, squares, circles represent the experimental data with error bars in $2n$, $3n$, and $4n$ evaporation channels, respectively. The experimental data are obtained from Refs. [24,25,60,61].

of great interest in the experiment, the calculations are also pretty close to the experimental data. It can be found that the maximum ER cross section is in the $3n$ or $4n$ evaporation channels. That is because the transmission and fusion probability is pretty low due to the low incident energy in $1n$ and $2n$ evaporation channels, and in the $5n$ evaporation channel, fission becomes the main de-excitation mode because of the high excitation energy.

Within the DNS model, fusion-evaporation reactions can be divided into three stages: capture, fusion, and de-excitation processes. The reactions $^{32,34,36}\text{S} + ^{255}\text{Es}$ are selected to analyze the influence of isospin of projectile on the three processes in fusion-evaporation reactions. Figures 3(a) and 3(b) shows the $V + Q$ values and capture cross sections, respectively. The $V_b + Q$ values of the three reactions are 46.70, 39.42, and 34.71 MeV, respectively. It can be found that the capture cross sections increase rapidly with the increase of incident energy. As the excitation energy reaches $V_b + Q$, the capture cross section almost tends to be a maximum. At that stage, the incident energy is just near the Coulomb barrier, and the quantum tunneling effect is obvious. As the excitation

energy is higher than $V_b + Q$, the capture cross sections still increase slowly with the increase of excitation energy. That enhancement comes from the partial cross sections at the larger angular momentum. It can be seen that $^{36}\text{S} + ^{255}\text{Es}$ reaction has the smallest $V_b + Q$ value among the three reactions, so its capture cross sections reach the maximum value at the lowest excitation energy compared with the other two reactions. Reactions with smaller $V_b + Q$ values would have an appreciable value of the capture cross section even in the low excitation energy region.

Figure 4(a) shows the driving potential as a function of the mass asymmetry η , defined as $\eta = (A_1 - A_2)/(A_1 + A_2)$, in $^{32}\text{S} + ^{255}\text{Es}$, $^{34}\text{S} + ^{255}\text{Es}$, and $^{36}\text{S} + ^{255}\text{Es}$ reactions, represented by solid, dashed, and dotted lines, respectively. It can be found that the inner fusion barrier in the $^{32}\text{S} + ^{255}\text{Es}$ reaction is the lowest because its mass asymmetry in the entrance channel is the largest among the three reactions. From Figure 4(b), one can notice that the fusion probability strongly depends on the excitation energy. As the excitation energy becomes higher, the fusion probability increases rapidly and reaches the maximum. The fusion probability in

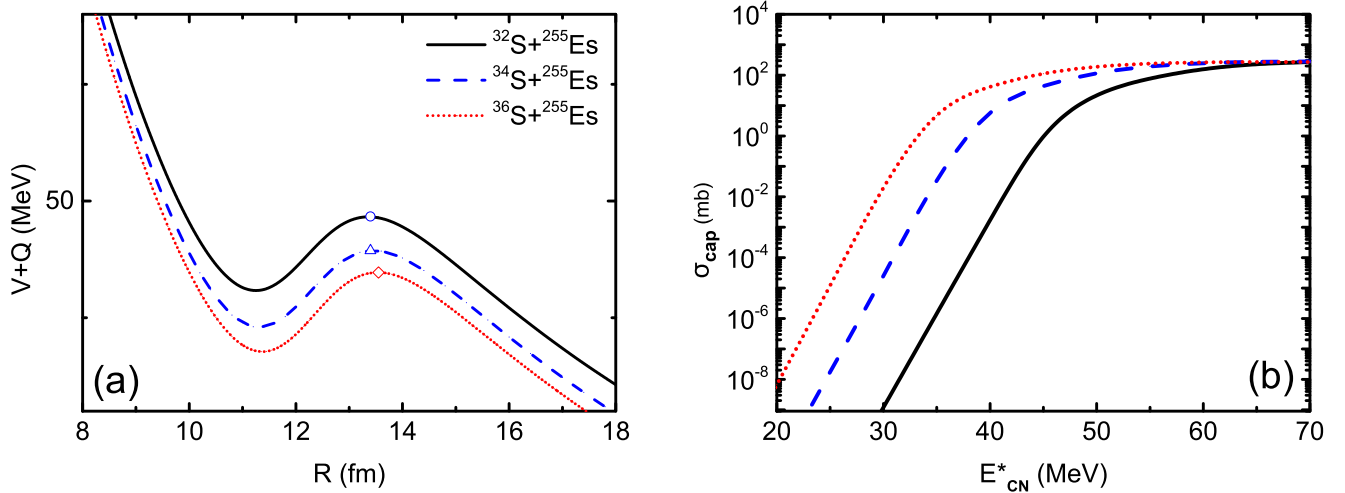


FIG. 3. (a) The $V + Q$ values in $^{32}\text{S} + ^{255}\text{Es}$, $^{34}\text{S} + ^{255}\text{Es}$, and $^{36}\text{S} + ^{255}\text{Es}$ reactions. The positions of Coulomb barrier are marked with open circle, triangle, and diamond. (b) The calculated capture cross sections in $^{32}\text{S} + ^{255}\text{Es}$, $^{34}\text{S} + ^{255}\text{Es}$, and $^{36}\text{S} + ^{255}\text{Es}$ reactions, denoted by the solid, dashed, and dotted lines, respectively.

the $^{32}\text{S} + ^{255}\text{Es}$ reaction is the highest due to the lowest inner barrier. A higher inner fusion barrier can strongly hinder the fusion process, resulting in a lower fusion probability. However, the maximum fusion probability of the three reactions is still rather small because quasifission accounts for the main contribution to the fusion process. It can be seen from Fig. 4(a) that the system is easier to develop towards the direction of small mass asymmetry corresponding to the quasifission process.

In Fig. 5(a), the survival probability in $^{32}\text{S} + ^{255}\text{Es}$, $^{34}\text{S} + ^{255}\text{Es}$, and $^{36}\text{S} + ^{255}\text{Es}$ reactions is shown, denoted by solid, dashed, and dash-dotted lines, respectively. The $p1n$, $p2n$, $p3n$, and $p4n$ channels are indicated by the black, red, blue, and pink lines, respectively. It is obvious that the survival probability is larger for the compound nucleus with more neutrons because its fission barrier is higher as shown in Fig. 5(b). At the same time, the peak values of survival

probability decrease rapidly with the increase in the number of evaporated particles. That is because the fission barrier of the compound nucleus decreases rapidly with the increase of excitation energy, and fission plays a more important role at higher excitation energy during the de-excitation process.

The ER cross sections in $^{36}\text{S} + ^{255}\text{Es}$, $^{48}\text{Ca} + ^{243}\text{Am}$, $^{48}\text{Ca} + ^{244}\text{Am}$, and $^{54}\text{Cr} + ^{239}\text{Pa}$ reactions for producing FI isotopes are shown in Fig. 6. The solid, dashed, dash-dotted, and dotted lines represent $p1n$, $p2n$, $p3n$, and $p4n$ evaporation channels, respectively. Comparing the reactions $^{36}\text{S} + ^{255}\text{Es}$ and $^{48}\text{Ca} + ^{243}\text{Am}$ with the same compound nucleus, one can find that the ER cross sections in the $^{36}\text{S} + ^{255}\text{Es}$ reaction are much larger than those in the $^{48}\text{Ca} + ^{243}\text{Am}$ reaction. That is because the mass asymmetry in $^{36}\text{S} + ^{255}\text{Es}$ reaction is larger, leading to a higher fusion probability. However, no unknown FI isotopes are produced in both reactions. Hence, the reactions $^{48}\text{Ca} + ^{244}\text{Am}$ and $^{54}\text{Cr} + ^{239}\text{Pa}$ are chosen to

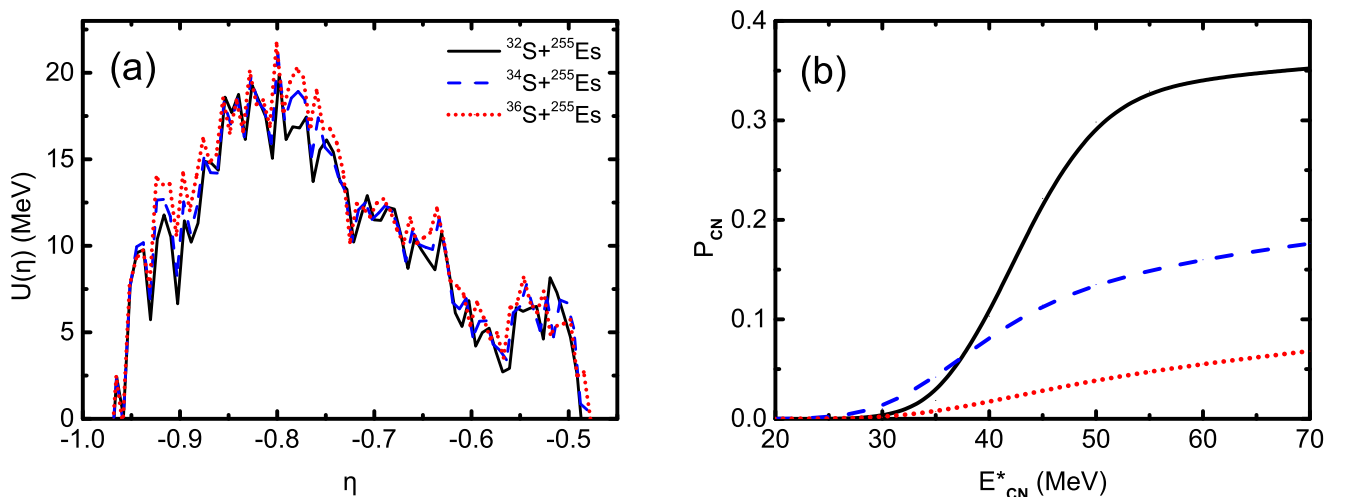


FIG. 4. (a) The driving potential as a function of the mass asymmetry η in $^{32}\text{S} + ^{255}\text{Es}$, $^{34}\text{S} + ^{255}\text{Es}$, and $^{36}\text{S} + ^{255}\text{Es}$ reactions, represented by solid, dashed, and dotted lines, respectively. (b) The fusion probability in $^{32}\text{S} + ^{255}\text{Es}$, $^{34}\text{S} + ^{255}\text{Es}$, and $^{36}\text{S} + ^{255}\text{Es}$ reactions.

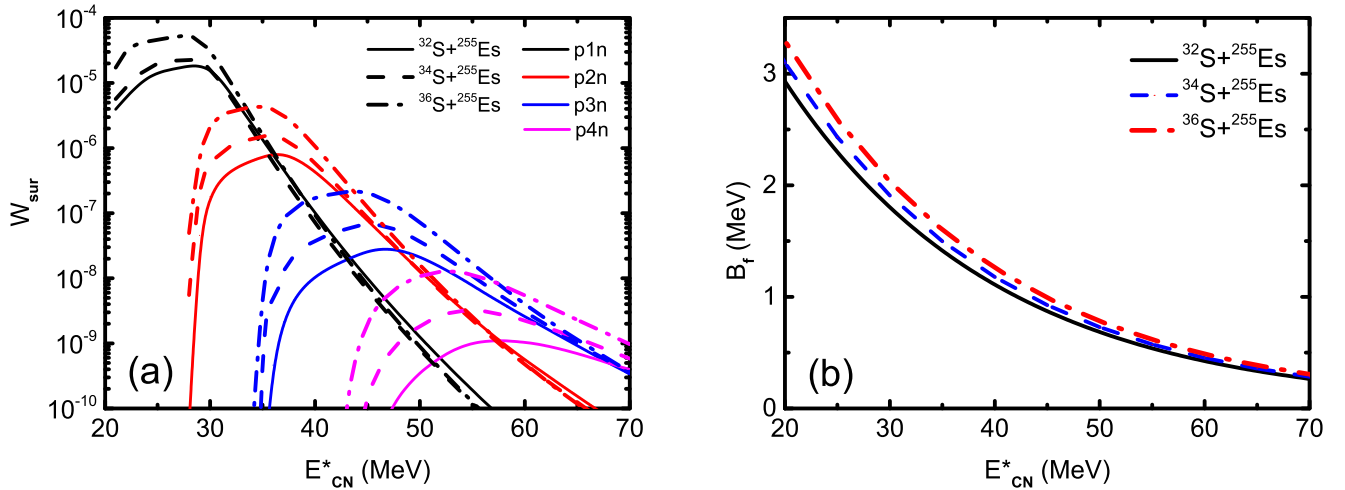


FIG. 5. (a) The survival probability in $^{32}\text{S} + ^{255}\text{Es}$, $^{34}\text{S} + ^{255}\text{Es}$, and $^{36}\text{S} + ^{255}\text{Es}$ reactions, denoted by solid, dashed, and dash-dotted lines, respectively. The $p1n$, $p2n$, $p3n$, and $p4n$ channels are indicated by the black, red, blue, and pink lines, respectively. (b) The fission barrier of compound nucleus formed by reactions $^{32}\text{S} + ^{255}\text{Es}$, $^{34}\text{S} + ^{255}\text{Es}$, and $^{36}\text{S} + ^{255}\text{Es}$ are represented by solid, dashed, and dash-dotted lines, respectively.

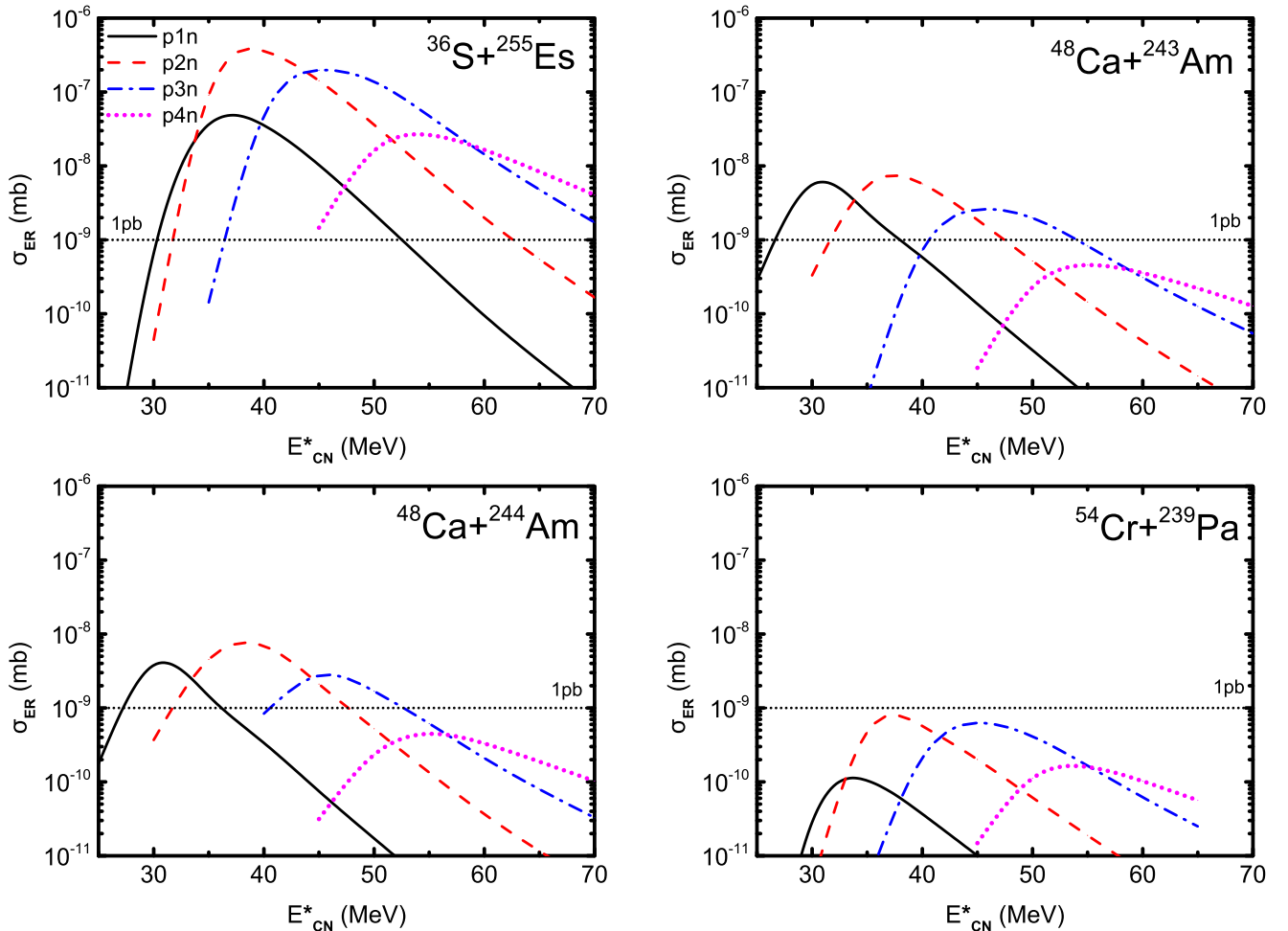


FIG. 6. Comparisons of calculated ER cross sections in $^{36}\text{S} + ^{255}\text{Es}$, $^{48}\text{Ca} + ^{243}\text{Am}$, $^{48}\text{Ca} + ^{244}\text{Am}$, and $^{54}\text{Cr} + ^{239}\text{Pa}$ reactions. Solid, dashed, dash-dotted, and dotted lines represent $p1n$, $p2n$, $p3n$, and $p4n$ evaporation channels, respectively.

TABLE I. Uncertainty of predictions. Indicated with an asterisk “*” are unknown isotopes.

Reaction	Isotope	E_{CN}^* (MeV)	σ_{max} (pb)
$^{36}\text{S} + ^{255}\text{Es} (p1n)$	^{289}Fl	37.2	$48.6^{+11.63}_{-8.21}$
$^{36}\text{S} + ^{255}\text{Es} (p2n)$	^{288}Fl	$38.8^{+0.11}_{-0.11}$	$387.1^{+148.3}_{-105.7}$
$^{36}\text{S} + ^{255}\text{Es} (p3n)$	^{287}Fl	$45.5^{+0.41}_{-0.3}$	$197.6^{+98.8}_{-64.7}$
$^{36}\text{S} + ^{255}\text{Es} (p4n)$	^{286}Fl	$53.8^{+0.06}_{-0.47}$	$26.9^{+15.4}_{-9.5}$
$^{48}\text{Ca} + ^{243}\text{Am} (p1n)$	^{289}Fl	30.9	$5.9^{+1.84}_{-1.15}$
$^{48}\text{Ca} + ^{243}\text{Am} (p2n)$	^{288}Fl	$37.3^{+0.1}_{-0.1}$	$7.3^{+3.1}_{-2.0}$
$^{48}\text{Ca} + ^{243}\text{Am} (p3n)$	^{287}Fl	$45.8^{+0.3}_{-0.5}$	$2.6^{+1.3}_{-0.8}$
$^{48}\text{Ca} + ^{243}\text{Am} (p4n)$	^{286}Fl	$55.1^{+0.4}_{-0.6}$	$0.5^{+0.2}_{-0.2}$
$^{54}\text{Cr} + ^{239}\text{Pa} (p1n)$	$^{291}\text{Fl}^*$	33.6	$0.11^{+0.03}_{-0.03}$
$^{54}\text{Cr} + ^{239}\text{Pa} (p2n)$	$^{290}\text{Fl}^*$	$37.2^{+0.12}_{-0.2}$	$0.8^{+0.3}_{-0.3}$
$^{54}\text{Cr} + ^{239}\text{Pa} (p3n)$	^{289}Fl	$45.1^{+0.2}_{-0.7}$	$0.6^{+0.4}_{-0.3}$
$^{54}\text{Cr} + ^{239}\text{Pa} (p4n)$	^{288}Fl	$53.4^{+0.3}_{-1.5}$	$0.2^{+0.1}_{-0.1}$
$^{48}\text{Ca} + ^{244}\text{Am} (p1n)$	$^{290}\text{Fl}^*$	30.9	$4.03^{+1.14}_{-0.85}$
$^{48}\text{Ca} + ^{244}\text{Am} (p2n)$	^{289}Fl	$38.4^{+0.1}_{-0.1}$	$7.6^{+3.1}_{-2.2}$
$^{48}\text{Ca} + ^{244}\text{Am} (p3n)$	^{288}Fl	$45.8^{+0.1}_{-0.2}$	$2.8^{+1.5}_{-0.9}$
$^{48}\text{Ca} + ^{244}\text{Am} (p4n)$	^{287}Fl	$55.4^{+0.5}_{-0.4}$	$0.5^{+0.2}_{-0.2}$

predict the production of new Fl isotopes. It can be found that one unknown isotope, ^{290}Fl , can be produced in the $p1n$ evaporation channel in the $^{48}\text{Ca} + ^{244}\text{Am}$ reaction with maximum ER cross section of 4.07 pb at $E_{CN}^* = 30.9$ MeV. In the reaction $^{54}\text{Cr} + ^{239}\text{Pa}$, more unknown Fl isotopes, $^{290,291}\text{Fl}$, can be generated in $p2n$ and $p1n$ channels with maximum ER cross sections of 0.78 pb and 0.11 pb at $E_{CN}^* = 37.3$ MeV and 33.7 MeV, respectively. The isotope ^{290}Fl is produced in $^{48}\text{Ca} + ^{244}\text{Am}$ and $^{54}\text{Cr} + ^{239}\text{Pa}$ reactions, while the ER cross sections in $^{48}\text{Ca} + ^{244}\text{Am}$ reaction are larger due to the lower Coulomb barrier and higher mass asymmetry. Therefore, the $^{48}\text{Ca} + ^{244}\text{Am}$ reaction is suggested to produce the isotope ^{290}Fl and the reaction $^{54}\text{Cr} + ^{239}\text{Pa}$ is expected to synthesize the isotope ^{291}Fl .

Considering the sensitivity of the DNS model to certain parameters, it is necessary to evaluate the inaccuracy of theoretical calculations in order to find out the uncertainty of predictions. Among the parameters in the model, the shell damping factor E_d plays a vital role in the ER cross sections [28]. The shell damping factor cannot be precisely

determined both experimentally and theoretically, and its inaccuracy is considered based on the experimental data in Ref. [62]. The uncertainties of the optimal excitation energy and maximum ER cross sections in the four reactions are shown in Table I. It can be seen that the uncertainties of the production cross sections of Fl isotopes are no better than one order of magnitude, and the uncertainties of the optimal excitation energy are only in the order of 0.1 MeV.

IV. CONCLUSIONS

In summary, the production of Fl isotopes in proton evaporation channels is investigated within the DNS model. Among the isotopes around $Z = 114$, proton evaporation is the easiest for Mc isotopes but the most difficult for Fl isotopes due to the proton closed-shell at $Z = 114$. Hence, one can synthesize the Fl isotopes in the proton evaporation channel. The calculated ER cross sections by the DNS model reproduce the experimental data very well. The capture, fusion, and survival processes in $^{32,34,36}\text{S} + ^{255}\text{Es}$ reactions are investigated. The capture cross sections in $^{36}\text{S} + ^{255}\text{Es}$ reaction are the largest because of the smallest values of $V_b + Q$. In the fusion process, the fusion probability in the $^{32}\text{S} + ^{255}\text{Es}$ reaction is the highest, due to the largest mass asymmetry, leading to the lowest inner fusion barrier. The survival probability in the $^{36}\text{S} + ^{255}\text{Es}$ reaction is the largest because the fission barrier for the compound nucleus with most neutrons is the highest. The synthesis of Fl isotopes is studied via $^{36}\text{S} + ^{255}\text{Es}$, $^{48}\text{Ca} + ^{243}\text{Am}$, $^{48}\text{Ca} + ^{244}\text{Am}$, and $^{54}\text{Cr} + ^{239}\text{Pa}$ reactions. No unknown Fl isotopes are produced in $^{36}\text{S} + ^{255}\text{Es}$ and $^{48}\text{Ca} + ^{243}\text{Am}$ reactions. The reaction $^{48}\text{Ca} + ^{244}\text{Am}$ is more favorable to produce the unknown isotope ^{290}Fl than $^{54}\text{Cr} + ^{239}\text{Pa}$ reaction with maximal ER cross section of 4.07 pb. The unknown isotope ^{291}Fl can be synthesized in the $^{54}\text{Cr} + ^{239}\text{Pa}$ reaction in the $p1n$ evaporation channel with an estimated production cross section of 0.11 pb. The uncertainties of the predictions from the inaccuracy of the shell damping factor are calculated, and the uncertainties of the ER cross sections of Fl isotopes are no better than one order of magnitude.

ACKNOWLEDGMENTS

This work was supported by the Guangxi Natural Science Foundation under Grant No. 2022GXNSFBA035549.

- [1] S. Hofmann, V. Ninov, F. P. Heßberger, P. Armbruster, H. Folger, G. Münzenberg, H. J. Schött, A. G. Popeko, A. V. Yeremin, A. N. Andreyev, S. Saro, R. Janik, and M. Leino, *Z. Phys. A: Hadrons Nucl.* **350**, 277 (1995).
- [2] S. Hofmann, V. Ninov, F. P. Heßberger, P. Armbruster, H. Folger, G. Münzenberg, H. J. Schött, A. G. Popeko, A. V. Yeremin, A. N. Andreyev, S. Saro, R. Janik, and M. Leino, *Z. Phys. A: Hadrons Nucl.* **350**, 281 (1995).
- [3] S. Hofmann, V. Ninov, F. P. Heßberger, P. Armbruster, H. Folger, G. Münzenberg, H. J. Schött, A. G. Popeko, A. V. Yeremin, S. Saro, R. Janik, and M. Leino, *Z. Phys. A: Hadrons Nucl.* **354**, 229 (1996).

- [4] S. Hofmann and G. Münzenberg, *Rev. Mod. Phys.* **72**, 733 (2000).
- [5] K. Morita, K. Morimoto, D. Kaji, H. Haba, E. Ideguchi, R. Kanungo, K. Katori, H. Koura, H. Kudo, T. Ohnishi, A. Ozawa, T. Suda, K. Sueki, I. Tanihata, H. Xu, A. V. Yeremin, A. Yoneda, A. Yoshida, Y. L. Zhao, and T. Zheng, *Eur. Phys. J. A* **21**, 257 (2004).
- [6] Yu. Ts. Oganessian, V. K. Utyonkov, Yu. V. Lobanov, F. Sh. Abdullin, A. N. Polyakov, I. V. Shirokovsky, Yu. S. Tsyganov, G. G. Gulbekian, S. L. Bogomolov, B. N. Gikal, A. N. Mezentsev, S. Iliev, V. G. Subbotin, A. M. Sukhov, G. V. Buklanov, K. Subotic, M. G. Itkis, K. J. Moody, J. F. Wild, N. J.

- Stoyer, M. A. Stoyer, and R. W. Lougheed, *Phys. Rev. Lett.* **83**, 3154 (1999).
- [7] Yu. Ts. Oganessian, V. K. Utyonkov, Y. V. Lobanov, F. Sh. Abdullin, A. N. Polyakov, R. N. Sagaidak, I. V. Shirokovsky, Yu. S. Tsyganov, A. A. Voinov, G. G. Gulbekian, S. L. Bogomolov, B. N. Gikal, A. N. Mezentsev, S. Iliev, V. G. Subbotin, A. M. Sukhov, K. Subotic, V. I. Zagrebaev, G. K. Vostokin, M. G. Itkis, K. J. Moody, J. B. Patin *et al.*, *Phys. Rev. C* **74**, 044602 (2006).
- [8] Yu. Ts. Oganessian, F. Sh. Abdullin, P. D. Bailey, D. E. Benker, M. E. Bennett, S. N. Dmitriev, J. G. Ezold, J. H. Hamilton, R. A. Henderson, M. G. Itkis, Y. V. Lobanov, A. N. Mezentsev, K. J. Moody, S. L. Nelson, A. N. Polyakov, C. E. Porter, A. V. Ramayya, F. D. Riley, J. B. Roberto, M. A. Ryabinin, K. P. Rykaczewski, R. N. Sagaidak *et al.*, *Phys. Rev. Lett.* **104**, 142502 (2010).
- [9] Yu. Ts. Oganessian, *J. Phys. G* **787**, 343 (2007).
- [10] Yu. Ts. Oganessian and V. K. Utyonkov, *Nucl. Phys. A* **944**, 62 (2015).
- [11] W. Loveland, K. E. Gregorich, J. B. Patin, D. Peterson, C. Rouki, P. M. Zielinski, and K. Aleklett, *Phys. Rev. C* **66**, 044617 (2002).
- [12] S. Hofmann, D. Ackermann, S. Antalic, H. G. Burkhard, V. F. Comas, R. Dressler, Z. Gan, S. Heinz, J. A. Heredia, F. P. Heßberger, Khuyagbaatar, B. Kindler, I. Kojouharov, P. Kuusiniemi, M. Leino, B. Lommel, R. Mann, G. Münzenberg, K. Nishio, A. G. Popeko, S. Saro *et al.*, *Eur. Phys. J. A* **32**, 251 (2007).
- [13] L. Stavsetra, K. E. Gregorich, J. Dvorak, P. A. Ellison, I. Dragojević, M. A. Garcia, and H. Nitsche, *Phys. Rev. Lett.* **103**, 132502 (2009).
- [14] C. E. Düllmann, M. Schädel, A. Yakushev, A. Türler, K. Eberhardt, J. V. Kratz, D. Ackermann, L. L. Andersson, M. Block, W. Brühle, J. Dvorak, H. G. Essel, P. A. Ellison, J. Even, J. M. Gates, A. Gorshkov, R. Graeger, K. E. Gregorich, W. Hartmann, R. D. Herzberg *et al.*, *Phys. Rev. Lett.* **104**, 252701 (2010).
- [15] J. M. Gates, C. E. Düllmann, M. Schädel, A. Yakushev, A. Türler, K. Eberhardt, J. V. Kratz, D. Ackermann, L. L. Andersson, M. Block, W. Brühle, J. Dvorak, H. G. Essel, P. A. Ellison, J. Even, U. Forsberg, J. Gellanki, A. Gorshkov, R. Graeger, K. E. Gregorich *et al.*, *Phys. Rev. C* **83**, 054618 (2011).
- [16] S. Hofmann, S. Heinz, R. Mann, J. Maurer, J. Khuyagbaatar, D. Ackermann, S. Antalic, W. Barth, M. Block, H. G. Burkhard, V. F. Comas, L. Dahl, K. Eberhardt, J. Gostic, R. A. Henderson, J. A. Heredia, F. P. Heßberger, J. M. Kenneally, B. Kindler, I. Kojouharov *et al.*, *Eur. Phys. J. A* **48**, 62 (2012).
- [17] J. Khuyagbaatar, A. Yakushev, C. E. Düllmann, D. Ackermann, L.-L. Andersson, M. Asai, M. Block, R. A. Boll, H. Brand, D. M. Cox, M. Dasgupta, X. Derkx, A. Di Nitto, K. Eberhardt, J. Even, M. Evers, C. Fahlander, U. Forsberg, J. M. Gates, N. Gharibyan, P. Golubev *et al.*, *Phys. Rev. Lett.* **112**, 172501 (2014).
- [18] V. K. Utyonkov, N. T. Brewer, Yu. Ts. Oganessian, K. P. Rykaczewski, F. Sh. Abdullin, S. N. Dmitriev, R. K. Grzywacz, M. G. Itkis, K. Miernik, A. N. Polyakov, J. B. Roberto, R. N. Sagaidak, I. V. Shirokovsky, M. V. Shumeiko, Yu. S. Tsyganov, A. A. Voinov, V. G. Subbotin, A. M. Sukhov, A. V. Karpov, A. G. Popeko, A. V. Sabel'nikov, A. I. Svirikhin *et al.*, *Phys. Rev. C* **97**, 014320 (2018).
- [19] S. Ćwiok, J. Dobaczewski, P. H. Heenen, P. Magierski, and W. Nazarewicz, *Nucl. Phys. A* **611**, 211 (1996).
- [20] A. T. Kruppa, M. Bender, W. Nazarewicz, P.-G. Reinhard, T. Vertse, and S. Ćwiok, *Phys. Rev. C* **61**, 034313 (2000).
- [21] K. Rutz, M. Bender, T. Bürvenich, T. Schilling, P.-G. Reinhard, J. A. Maruhn, and W. Greiner, *Phys. Rev. C* **56**, 238 (1997).
- [22] S. Goriely, N. Chamel, and J. M. Pearson, *Phys. Rev. C* **88**, 061302(R) (2013).
- [23] Yu. Ts. Oganessian, V. K. Utyonkov, Yu. V. Lobanov, F. Sh. Abdullin, A. N. Polyakov, I. V. Shirokovsky, Yu. S. Tsyganov, G. G. Gulbekian, S. L. Bogomolov, B. N. Gikal, A. N. Mezentsev, S. Iliev, V. G. Subbotin, A. M. Sukhov, O. V. Ivanov, G. V. Buklanov, K. Subotic, M. G. Itkis, K. J. Moody, J. F. Wild, N. J. Stoyer, M. A. Stoyer *et al.*, *Phys. Rev. C* **62**, 041604(R) (2000).
- [24] Yu. Ts. Oganessian, V. K. Utyonkov, Yu. V. Lobanov, F. Sh. Abdullin, A. N. Polyakov, I. V. Shirokovsky, Yu. S. Tsyganov, G. G. Gulbekian, S. L. Bogomolov, A. N. Mezentsev, S. Iliev, V. G. Subbotin, A. M. Sukhov, A. A. Voinov, G. V. Buklanov, K. Subotic, V. I. Zagrebaev, M. G. Itkis, J. B. Patin, K. J. Moody, J. F. Wild, M. A. Stoyer *et al.*, *Phys. Rev. C* **69**, 021601(R) (2004).
- [25] Yu. Ts. Oganessian, V. K. Utyonkov, Yu. V. Lobanov, F. Sh. Abdullin, A. N. Polyakov, I. V. Shirokovsky, Yu. S. Tsyganov, G. G. Gulbekian, S. L. Bogomolov, B. N. Gikal, A. N. Mezentsev, S. Iliev, V. G. Subbotin, A. M. Sukhov, A. A. Voinov, G. V. Buklanov, K. Subotic, V. I. Zagrebaev, M. G. Itkis, J. B. Patin, K. J. Moody, J. F. Wild *et al.*, *Phys. Rev. C* **70**, 064609 (2004).
- [26] V. K. Utyonkov, N. T. Brewer, Yu. Ts. Oganessian, K. P. Rykaczewski, F. Sh. Abdullin, S. N. Dmitriev, R. K. Grzywacz, M. G. Itkis, K. Miernik, A. N. Polyakov, J. B. Roberto, R. N. Sagaidak, I. V. Shirokovsky, M. V. Shumeiko, Yu. S. Tsyganov, A. A. Voinov, V. G. Subbotin, A. M. Sukhov, A. V. Sabel'nikov, G. K. Vostokin, J. H. Hamilton, M. A. Stoyer *et al.*, *Phys. Rev. C* **92**, 034609 (2015).
- [27] Yu. S. Tsyganov, *J. Phys. G: Nucl. Part. Phys.* **25**, 937 (1999).
- [28] H. L. Lü, D. Boilley, Y. Abe, and C. W. Shen, *Phys. Rev. C* **94**, 034616 (2016).
- [29] D. Boilley, H. L. Lü, C. W. Shen, Y. Abe, and B. G. Giraud, *Phys. Rev. C* **84**, 054608 (2011).
- [30] Y. Abe, C. Shen, D. Boilley, B. G. Giraud, and G. Kosenko, *Nucl. Phys. A* **834**, 349c (2010).
- [31] G. G. Adamian, N. V. Antonenko, W. Scheid, and V. V. Volkov, *Nucl. Phys. A* **633**, 409 (1998).
- [32] A. K. Nasirov, G. Mandaglio, M. Mangano, A. I. Muminov, G. Fazio, and G. Giardina, *Phys. Lett. B* **686**, 72 (2010).
- [33] A. K. Nasirov, G. Mandaglio, G. Giardina, A. Sobiczewski, and A. I. Muminov, *Phys. Rev. C* **84**, 044612 (2011).
- [34] A. K. Nasirov, B. M. Kayumov, G. Mandaglio, G. Giardina, K. Kim, and Y. Kim, *Eur. Phys. J. A* **55**, 29 (2019).
- [35] Z. Q. Feng, G. M. Jin, and J. Q. Li, *Phys. Rev. C* **80**, 057601 (2009).
- [36] L. Zhu, W. J. Xie, and F. S. Zhang, *Phys. Rev. C* **89**, 024615 (2014).
- [37] C. Shen, G. Kosenko, and Y. Abe, *Phys. Rev. C* **66**, 061602(R) (2002).
- [38] V. I. Zagrebaev, *Phys. Rev. C* **64**, 034606 (2001).
- [39] Z. H. Liu and J. D. Bao, *Phys. Rev. C* **80**, 054608 (2009).
- [40] V. Zagrebaev and W. Greiner, *Phys. Rev. C* **78**, 034610 (2008).
- [41] K. Sekizawa and K. Yabana, *Phys. Rev. C* **93**, 054616 (2016).

- [42] J. Tian, X. Wu, K. Zhao, Y. Zhang, and Z. Li, *Phys. Rev. C* **77**, 064603 (2008).
- [43] C. Li, F. Zhang, J. J. Li, L. Zhu, J. L. Tian, N. Wang, and F. S. Zhang, *Phys. Rev. C* **93**, 014618 (2016).
- [44] Z. Q. Feng, G. M. Jin, F. Fu, and J. Q. Li, *Nucl. Phys. A* **771**, 50 (2006).
- [45] G. G. Adamian, N. V. Antonenko, and W. Scheid, *Nucl. Phys. A* **618**, 176 (1997).
- [46] C. Y. Wong, *Phys. Rev. Lett.* **31**, 766 (1973).
- [47] G. G. Adamian, N. V. Antonenko, and R. V. Jolos, *Int. J. Mod. Phys. E* **05**, 191 (1996).
- [48] S. Ayik, B. Schürmann, and W. Nürenberg, *Z. Phys. A* **277**, 299 (1976).
- [49] L. Zhu, F. S. Zhang, P. W. Wen, J. Su, and W. J. Xie, *Phys. Rev. C* **96**, 024606 (2017).
- [50] P. Grangé, Jun-Qing Li, and H. A. Weidenmüller, *Phys. Rev. C* **27**, 2063 (1983).
- [51] G. G. Adamian, N. V. Antonenko, and W. Scheid, *Phys. Rev. C* **68**, 034601 (2003).
- [52] G. Wolschin and W. Nürenberg, *Z. Phys. A* **284**, 209 (1978).
- [53] V. Weisskopf, *Phys. Rev.* **52**, 295 (1937).
- [54] N. Bohr and J. A. Wheeler, *Phys. Rev.* **56**, 426 (1939).
- [55] A. S. Zubov, G. G. Adamian, N. V. Antonenko, S. P. Ivanova, and W. Scheid, *Phys. Rev. C* **68**, 014616 (2003).
- [56] J. Hong, G. G. Adamian, and N. V. Antonenko, *Phys. Rev. C* **94**, 044606 (2016).
- [57] P. H. Chen, Z. Q. Feng, F. Niu, Y. F. Guo, H. F. Zhang, J. Q. Li, and G. M. Jin, *Eur. Phys. J. A* **53**, 95 (2017).
- [58] J. D. Jackson, *Can. J. Phys.* **34**, 767 (1956).
- [59] J. Hong, G. G. Adamian, N. V. Antonenko, P. Jachimowicz, and M. Kowal, *Phys. Lett. B* **809**, 135760 (2020).
- [60] Yu. Ts. Oganessian, F. Sh. Abdullin, S. N. Dmitriev, J. M. Gostic, J. H. Hamilton, R. A. Henderson, M. G. Itkis, K. J. Moody, A. N. Polyakov, A. V. Ramayya, J. B. Roberto, K. P. Rykaczewski, R. N. Sagaidak, D. A. Shaughnessy, I. V. Shirokovsky, M. A. Stoyer, V. G. Subbotin, A. M. Sukhov, Yu. S. Tsyganov, V. K. Utyonkov, A. A. Voinov, and G. K. Vostokin, *Phys. Rev. Lett.* **108**, 022502 (2012).
- [61] Yu. Ts. Oganessian and V. K. Utyonkov, *Rep. Prog. Phys.* **78**, 036301 (2015).
- [62] P. C. Rout, D. R. Chakrabarty, V. M. Datar, S. Kumar, E. T. Mirgule, A. Mitra, V. Nanal, S. P. Behera, and V. Singh, *Phys. Rev. Lett.* **110**, 062501 (2013).